Spin-orbit coupling, Fermi surface, and optical conductivity of ferromagnetic iron*

M. Singh, C. S. Wang, and J. Callaway
Department of Physics and Astronomy, Louisiana State University, Baton Rouge, Louisiana 70803
(Received 30 May 1974)

A previous self-consistent linear-combination-of-atomic-orbitals calculation of energy bands in iron has been extended through the inclusion of spin-orbit coupling. The exchange interaction is incorporated according to the $X\alpha$ method. The Fermi surface is described in detail and compared with the results of measurements of the de Haas–van Alphen effect, and of magnetoresistance anisotropy. The interband contribution to the optical-conductivity tensor was computed using matrix elements determined from wave functions including spin-orbit coupling. Both diagonal and off-diagonal elements of this tensor have been obtained.

I. INTRODUCTION

This paper reports the extension of a previous band calculation for ferromagnetic iron[1] to include the effects of spin-orbit coupling. The present work includes a detailed comparison of Fermi-surface features with results of measurements of the de Haas–van Alphen effect,[2,3] and of the magnetoresistance anisotropy.[4,5] We have also computed the interband contribution to the optical-conductivity tensor and present results for both the diagonal and off-diagonal components of this tensor.

Spin-orbit coupling is of major significance in the determination of the Fermi surface and the optical properties of ferromagnetic transition metals. Bands of ↑ and ↓ spin are hybridized, and most of the accidental degeneracies which are present when spin-orbit coupling is neglected are removed. As a result, there can be substantial changes in the connectivity of the Fermi surface. The symmetry group of the crystal in the presence of ferromagnetic exchange and spin-orbit coupling is reduced in comparison with a state in which the possibility of spin polarization is neglected.[6,7] The conductivity tensor is not diagonal, and magneto-optical effects are produced.

We are not aware of a previous first-principles band calculation for iron which includes both exchange splitting and spin-orbit coupling. A model band structure has, however, been developed by Maglic and Mueller[8] in which spin-orbit coupling is added to an interpolation scheme based on the Korringa-Kohn-Rostoker (KKR) band calculation of Wakoh and Yamashita.[9] In the present work, the spin-orbit interaction is determined from the self-consistent potential used in the band calculation of Ref. 1. Our method has previously been applied to nickel,[10] and Ref. 10 can be consulted for details not contained here. Our results show some differences in the effect of spin-orbit coupling on the Fermi surface in comparison with Ref. 8.

The plan of this paper is as follows. We summarize, in the remainder of this Introduction, the essential features of the calculation reported in Ref. 1 on which this work is based. Section II describes briefly the procedures of the band-structure calculation when spin-orbit coupling is included. The calculated Fermi surface is discussed, and compared with experimental results in Sec. III. The computation of the conductivity tensor is presented in Sec. IV, and also compared with the available experimental information.

The band calculation described in Ref. 1 employed the tight-binding method as reformulated by LaFon and Lin.[11] The basis set consisted of atomic wave functions for all states except $3d$ ($1s$, $2s$, $3s$, $4s$, $2p$, $3p$, and $4p$) expressed as linear combinations of Gaussian-type orbitals (GTO) determined by Wachters[12] from a self-consistent-field calculation for the free iron atom. Five independent GTO were introduced for each of the five $l=2$ angular functions. The orbital exponents used in defining these functions were the same as employed by Wachters. Exchange was included according to the $X\alpha$ approximation.[13] The coefficient of the Slater-exchange potential was taken as $\alpha=0.64$, slightly smaller than the Kohn-Sham-Gaspar[14] value ($\frac{2}{3}$) used in the case of nickel.[10] This choice was made so that the Fermi energy would be slightly below the energy of the majority spin level of symmetry $H_{25'}$, since the de Haas–van Alphen measurements indicate the presence of majority spin holes around H.[2,3] The Hamiltonian and overlap matrices are of dimension 38×38. Since a spin-polarized potential was employed, matrices for majority and minority spin states were diagonalized separately. The potential for the first iteration of the self-consistent calculation was obtained from the superposition of neutral-atom d^7s^1 charge densities. The essential techniques employed in the iterative procedure to achieve self-consistency have been described elsewhere.[1,15] The final iterations of the self-consistency procedure were made using a charge density determined from 140 points in $\frac{1}{48}$th

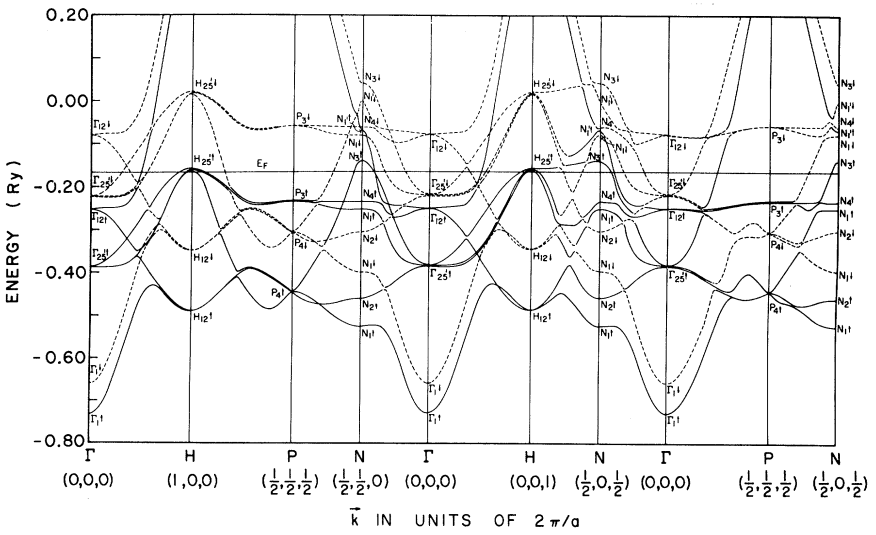

FIG. 1. Band structure of iron along some symmetry lines in the Brillouin zone. The spin alignment direction is [001]. States are labeled according to the symmetry of the larger spin component. The solid lines indicate states of predominately majority spin; the dashed lines, those of minority spin.

of the Brillouin zone. The criterion used for self-consistency was that the Fourier coefficients of the Coulomb potential should be stable to 0.001 Ry. The calculated energy levels were found to be in reasonable agreement with those obtained in the KKR calculation of Wakoh and Yamashita,[9] but we obtained a band narrower by a factor of approximately 2 than that reported by Duff and Das.[16] We will not repeat a detailed description of the results here.

II. BAND CALCULATION WITH SPIN-ORBIT COUPLING

The calculation previously described was extended by the inclusion of the spin-orbit (SO) interaction,

$$H_{so} = (\hbar/4m^2c^2)\vec{\sigma}\cdot(\nabla V\times\vec{p}). \tag{1}$$

Other relativistic effects were neglected. Inclusion of H_{so} couples states of ↑ and ↓ spin, and leads to a doubling of the size of the Hamiltonian matrix (in our case, 76×76). Moreover, the elements become complex. The resulting band structure depends on the direction of spin alignment. We made extensive computations of energy levels for an assumed [001] direction of spin alignment and considered a smaller number of $\vec{k}$ points for spins aligned along the [110], [111], and [211] directions.

The potential V appearing in (1) was that obtained in Ref. 1 from the self-consistent band calculation, expressed as a Fourier series

$$V(\vec{r}) = \sum_s V(\vec{K}_s)\, e^{i\vec{K}_s\cdot\vec{r}}. \tag{2}$$

The matrix elements of (1) were computed using the same Gaussian orbital basis set as in Ref. 1. Calculations previously made for nickel indicated that the only nonnegligible matrix elements of H_{so} are those in the p-p and d-d blocks with orbitals centered on the same atomic site (central cell). Some details concerning the representation of the spin-orbit Hamiltonian on the GTO basis can be found in Ref. 10.

If the actual spin-orbit interaction given by (1) is approximated in the usual way,

$$H_{so} = \xi\vec{L}\cdot\vec{S}, \tag{3}$$

with an "atomic" spin-orbit parameter ξ, the strength of spin-orbit coupling in the solid can be compared with that existing in the free atom. We used the atomic wave function of Wachters[12] to evaluate ξ [but using our potential (2)]. We found $\xi = 0.0043$ Ry, which is somewhat larger than the atomic value $\xi = 0.0035$ Ry.[17]

Energy levels were determined at 729 points in $\frac{1}{16}$th of the Brillouin zone for a [001] assumed direction of spin alignment. The calculated band structure is shown along certain symmetry lines in Fig. 1. Some energy levels at symmetry points are listed in Table I. Since the actual symmetry group for this problem does not permit a particularly informative classification of states we have labeled states at symmetry points in terms of the predominant component, that is, neglecting the mixing of components of majority and minority spin. This labeling is meaningful since spin-orbit coupling is small compared to the exchange splitting.

The band structure shown in Fig. 1 is, to a first approximation, the superposition of the majority and minority spin band structures computed separately in Ref. 1. The Fermi energies are almost identical. However, spin-orbit coupling removes most of the accidental degeneracies present in such a picture, and hybridizes states of opposite spin.

TABLE I. Energy levels at symmetry points (Ry).

Band	$\Gamma(0,0,0)$	$N(\frac{1}{2},\frac{1}{2},0)$	$N(\frac{1}{2},0,\frac{1}{2})$	$P(\frac{1}{2},\frac{1}{2},\frac{1}{2})$	$H(1,0,0)$
12	-0.0795 ($\Gamma_{12}\downarrow$)	0.0404 ($N_3\downarrow$)	0.0405 ($N_3\downarrow$)	0.5789 ($P_4\uparrow$)	0.5252 ($H_{15}\uparrow$)
11	-0.0796 ($\Gamma_{12}\downarrow$)	-0.0023 ($N_1,\downarrow$)	-0.0023 ($N_1,\downarrow$)	0.5768 ($P_4\uparrow$)	0.5187 ($H_{15}\uparrow$)
10	-0.2184 ($\Gamma_{25},\downarrow$)	-0.0616 ($N_4\downarrow$)	-0.0620 ($N_4\downarrow$)	-0.0593 ($P_3\downarrow$)	0.0215 ($H_{25},\downarrow$)
9	-0.2207 ($\Gamma_{25},\downarrow$)	-0.0700 ($N_1,\uparrow$)	-0.0700 ($N_1,\uparrow$)	-0.0593 ($P_3\downarrow$)	0.0190 ($H_{25},\downarrow$)
8	-0.2217 ($\Gamma_{25},\downarrow$)	-0.0809 ($N_1\downarrow$)	-0.0806 ($N_1\downarrow$)	-0.2341 ($P_3\uparrow$)	0.0164 ($H_{25},\downarrow$)
7	-0.2513 ($\Gamma_{12}\uparrow$)	-0.1403 ($N_3\uparrow$)	-0.1401 ($N_3\uparrow$)	-0.2342 ($P_3\uparrow$)	-0.1576 ($H_{25},\uparrow$)
6	-0.2521 ($\Gamma_{12}\uparrow$)	-0.2363 ($N_4\uparrow$)	-0.2367 ($N_4\uparrow$)	-0.3070 ($P_4\downarrow$)	-0.1601 ($H_{25},\uparrow$)
5	-0.3827 ($\Gamma_{25},\uparrow$)	-0.2526 ($N_1\uparrow$)	-0.2525 ($N_1\uparrow$)	-0.3072 ($P_4\downarrow$)	-0.1625 ($H_{25},\uparrow$)
4	-0.3847 ($\Gamma_{25},\uparrow$)	-0.3053 ($N_2\downarrow$)	-0.3052 ($N_2\downarrow$)	-0.3076 ($P_4\downarrow$)	-0.3481 ($H_{12}\downarrow$)
3	-0.3866 ($\Gamma_{25},\uparrow$)	-0.3990 ($N_1\downarrow$)	-0.3991 ($N_1\downarrow$)	-0.4458 ($P_4\uparrow$)	-0.3481 ($H_{12}\downarrow$)
2	-0.6592 ($\Gamma_1\downarrow$)	-0.4605 ($N_2\uparrow$)	-0.4605 ($N_2\uparrow$)	-0.4464 ($P_4\uparrow$)	-0.4896 ($H_{12}\uparrow$)
1	-0.7300 ($\Gamma_1\uparrow$)	-0.5272 ($N_1\uparrow$)	-0.5272 ($N_1\uparrow$)	-0.4470 ($P_4\uparrow$)	-0.4896 ($H_{12}\uparrow$)

In addition, the reduction of the symmetry group reduces the number of equivalent wave vectors in a star, so that energies at points such as $N(\frac{1}{2},\frac{1}{2},0)$ and $N(\frac{1}{2},0,\frac{1}{2})$ are no longer equal.

Our calculated energy band and Fermi surface are consistent with the group theoretical analysis of Falicov and Ruvalds[6] as extended by Cracknell.[7] The following points deserve comment. (i) Accidental degeneracies may be permitted in symmetry planes perpendicular to $\vec{B}$, but are not required (see Fig. 5, to be discussed subsequently). (ii) All degeneracies required by symmetry in the absence of spin-orbit coupling are removed (for example, Δ_5, Γ_{12}).

The density of states was computed using the Gilat-Raubenheimer method[18] in combination with an interpolation scheme as described in Ref. 10. The spin projected and total densities of states are shown in Figs. 2–4. The magneton number was found to be 2.29 which is to be compared with experimental values which are in the range 2.12–2.06 as deduced from measurements of the magnetization[19] and of the g (Ref. 20) or g' (Ref. 21) factors. The value of the density of states at the Fermi energy was determined to be 13.3 electrons/(atom Ry). Measurements of the low-temperature specific heat yield a value of 27.3 (Ref. 22) for this quantity.

III. FERMI SURFACE

Recent experiments[2–5] have enabled a fairly complete description of the Fermi surface of iron. In this section, we will compare our calculated Fermi surface with the experimental results. Most of our energy-level calculations were performed with the [001] axis as the direction of spin alignment, which implies that we should obtain a Fermi-surface cross section relevant to experiment only in the (001) plane. However, the Fermi energy should depend only very weakly on the direction of spin orientation. We repeated the level calculations for a sample of points lying in the (110) and (111) planes with the spin-alignment direction perpendicular to the plane. The energies so obtained did not produce Fermi-surface cross sections in those planes which differed significantly from those

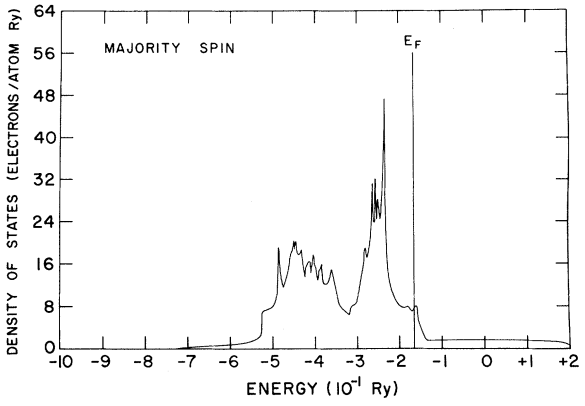

FIG. 2. Projected density of states for majority spin.

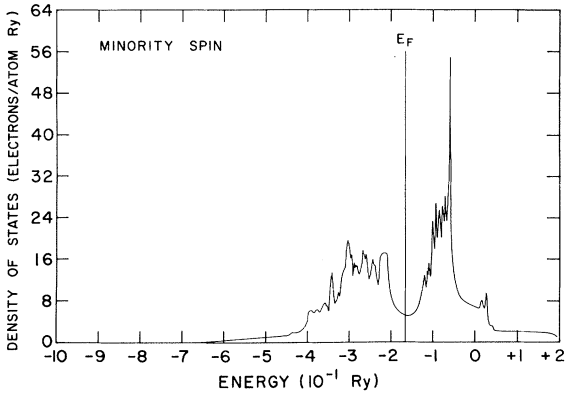

FIG. 3. Projected density of states for minority spin.

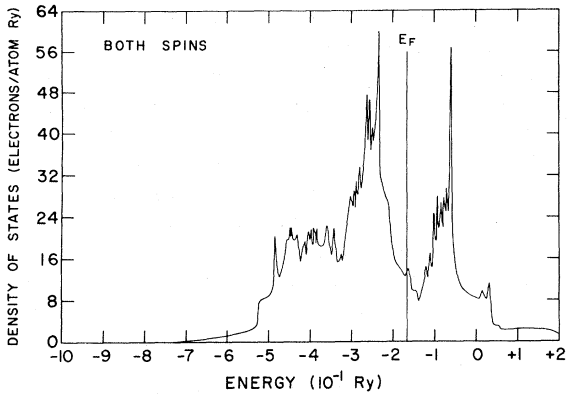

FIG. 4. Total density of states.

obtained in the same planes but with the field along [001]. Our calculated Fermi-surface cross sections are shown in Figs. 5–7. Numerical values for cross sections are given in Table II.

The Fermi surface calculated here is quite similar to that obtained in Ref. 1 except for some alterations caused by the removal of accidental degeneracies and some hybridization of states of different spins. There are eight pieces of Fermi surface (I–VIII) to be discussed.

(I). *Large electron surface centered about* Γ. This involves states of predominantly majority spin, except near *N* where there is some hybridization with minority spins. The calculated areas of the cross sections of this surface in the (100) and (110) planes are in good agreement with experiment. The calculated (111) cross section is slightly too small. The area in this plane is reduced from that predicted in the absence of spin-orbit coupling as a result of hybridization with a large predominantly minority spin hole pocket (VIII) near *N*.

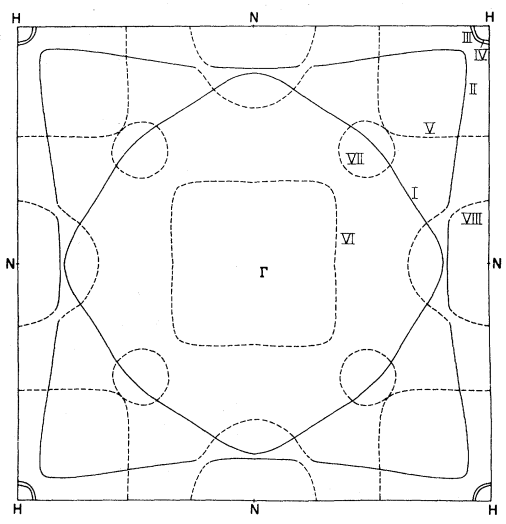

FIG. 5. Cross sections of the Fermi surface in the (100) plane. Portions of predominately majority spin are drawn with solid lines; predominately-minority-spin pieces are dashed. See text for labels.

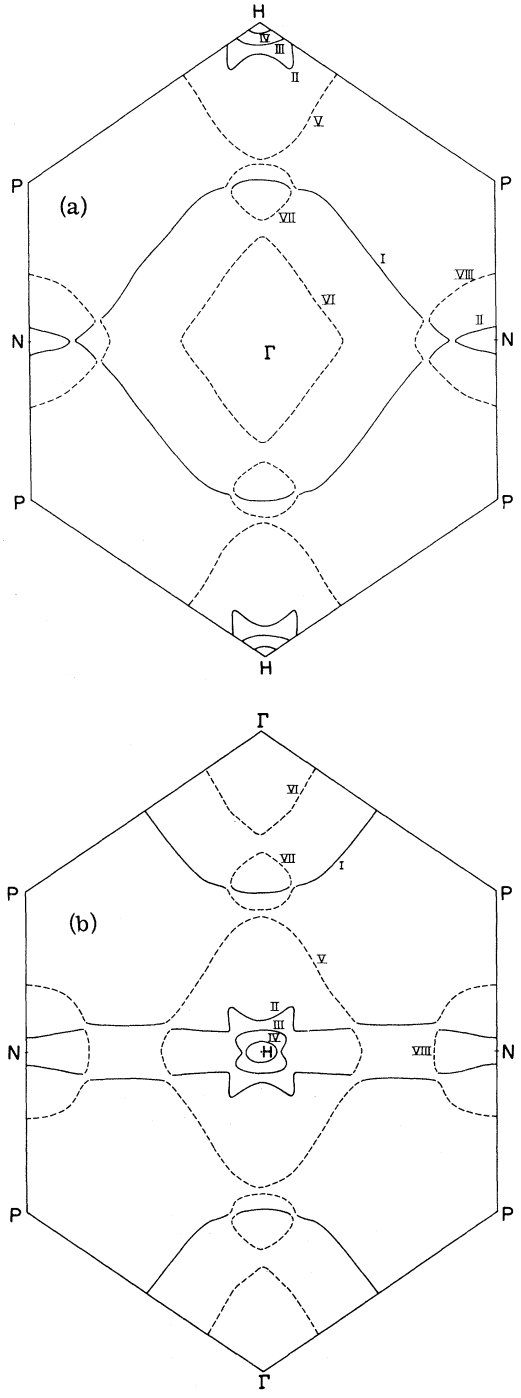

FIG. 6. Cross section of the Fermi surface in the (110) plane (a) centered about Γ and (b) centered about *H*.

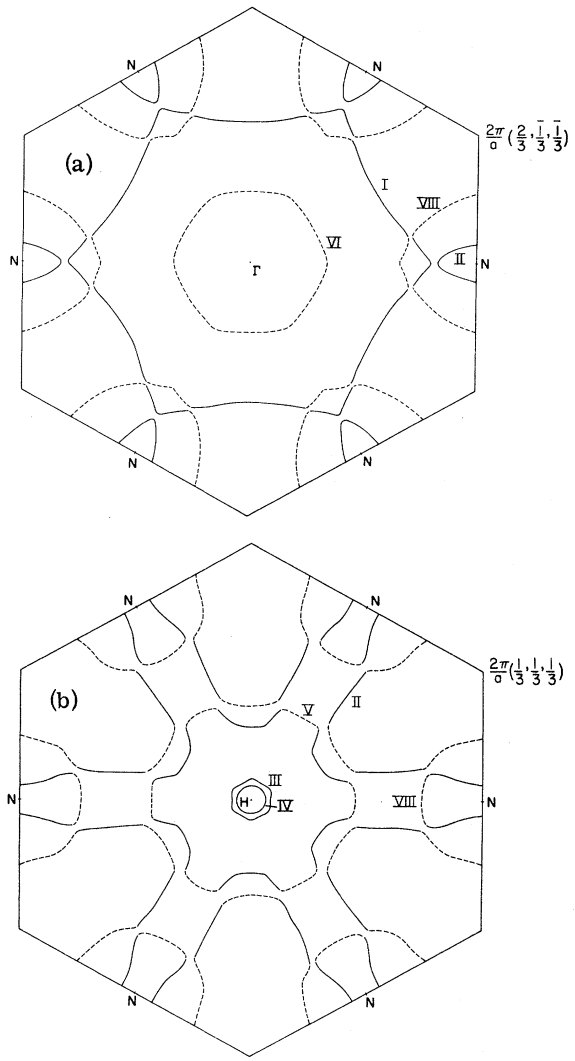

FIG. 7. Cross sections of the Fermi surface in (111) planes: (a) through Γ and (b), through *H*.

(II). *Major hole surface around H.* These arms extend in the *H-N* directions. In the (100) plane, the arms hybridize only with the hole ellipsoids around *N*, however, in the (110) and (111) planes there is an addition mixing with the large hole surface (V) around *H*. These latter surfaces do not mix in the (100) plane. This mixing leads to the possibility of open orbits in the [110] direction, which are required by the interpretation of magnetoresistance experiments.[4,5]

(III) and (IV). *Intermediate and small hole pockets about H.* These involve states of majority spin. Our calculated values for the cross sections of these pockets are uniformly much smaller than the values attributed to them in the interpretation of the de Haas–van Alphen measurements. This indicates that our calculated position of the level $H_{25'_1}$ is too close to the Fermi energy.

(V). *Large hole surface around H.* This is composed mainly of minority spin states. The cross sections of this surface are closed in the (100) and (111) planes; however, we find that hybridization with the hole arms in the (110) plane leads to open curves. Since closed orbits around this surface are actually observed in this plane, we conclude that magnetic breakdown must occur across a small gap produced by spin-orbit coupling. A reasonable degree of agreement between theory and experiment in regard to cross-sectional areas is found. The calculated cross section in the (111) plane is somewhat too small, whereas the calculation without spin-orbit coupling gives a result in substantially closer agreement with experiment. It is possible that magnetic breakdown restores an orbit similar to that calculated in the absence of spin-orbit coupling. There is actually no contact between surface (V) and the electron ball (VII), but the separation is too small to show in Fig. 5.

(VI). *Central (minority spin) electron surface about* Γ. Our results for the cross-sectional areas of this surface are consistently larger than the experimental values.

(VII). *Electron ball (minority spin) along* Δ. Our calculations predict a small ball which almost touches the hole octahedron (V) whereas the de Haas–van Alphen measurements indicate that the ball is larger and intersects the central minority spin surface. This is one of the most serious disagreements between our calculation and experiment. If the spin splitting were reduced by approximately 0.05 Ry, this surface would have approximately the correct shape and size. This would permit magnetic breakdown between surfaces III and V when the field is along the [112] direction, as is observed.[3] The dimensions of the hole pockets (III and IV) near *H* would also be improved. In addition, the somewhat too-large value we obtain for the magneton number would be reduced, although the amount of this reduction (to 1.98) is too large. We do not find any hybridization in the (100) plane between the electron ball and surface I, although mixing is present in other planes.

(VIII). *Hole pockets around N.* These surfaces are predicted by our calculation and some other first-principles studies.[9,23] They are composed of both majority and minority spin states. Spin-orbit coupling causes a marked reduction in the size of these surfaces through hybridization with the hole arms (II). The existence and properties of these pockets depends on the relative position of the *p*- and *d*-like levels near *N*. However, our basis set is probably more adequate for *d* states than for those of *p* symmetry and it is possible that a calculation in which separated orbitals rather than atomic functions were employed for states of *p* symme-

TABLE II. Predicted de Haas–van Alphen frequencies (in mG) compared with calculations without spin-orbit coupling (Ref. 1) and with experiment (Refs. 2 and 3).

Plane	Surface	Present result	Reference 1	Expt. Reference 2	Expt. Reference 3 (±1%)
(100)	I	433	421		436
	II	321	267		
	III	5.1	5.5	23.8	20.6
	IV	3.5	4.6	21.0	15.0
	V	218	219		198
	VI	120	119		71
	VII	11.0	11.0		37
	VIII	43	72		
(110)	I	349	347	347	349
	II (around *N*)	8.4	8.4		
	II (around *H*)	55	20		
	III	8.4	8.2		33.4
	IV	2.8	3.7	12.0	12.3
	V with breakdown	167	172		145
	VI	89	92		58
	VII	7.9	12.4		
	VIII through Γ	63	70		34
	VIII through *H*	23	65		
(111)	I	346	370	369±4	370
	II through Γ	10.0	9.6		
	II through *H*	207	282		
	III	6.15	9.9	28.0	27.0
	IV	2.97	4.4	11.3	11.4
	V	115	162	154	157
	VI	84	69	51.8	52.2
	VIII through Γ	65	72		
	VIII through *H*	25	61		

try might lead to some reordering of levels.

The magnetoresistance measurements indicate clearly the presence of open orbits in the [100] and [110] directions.[4,5] It was pointed out above that our model of the Fermi surface provides for such orbits in the [110] direction. To obtain open orbits in the [100] direction it is necessary for us to suppose that magnetic breakdown establishes paths close to the (100) plane involving surfaces II and V (or V, VII, and I). Additional open orbits in the [110] direction can be established similarly. Since we do not obtain overlap of the electron ball (VII) and the central electron surface (VI), we do not have as obvious a mechanism for the [100] orbits as is present in the model of Gold *et al.*[2] Further, we have no evident explanation for the apparent pressure dependence of the [100] open orbits.[5]

IV. OPTICAL CONDUCTIVITY

We have calculated the optical conductivity for iron by the same procedures employed in our previous calculation concerning nickel.[10] Both the diagonal and off-diagonal elements of the conductivity tensor were obtained. The $\vec{k}$ dependence of

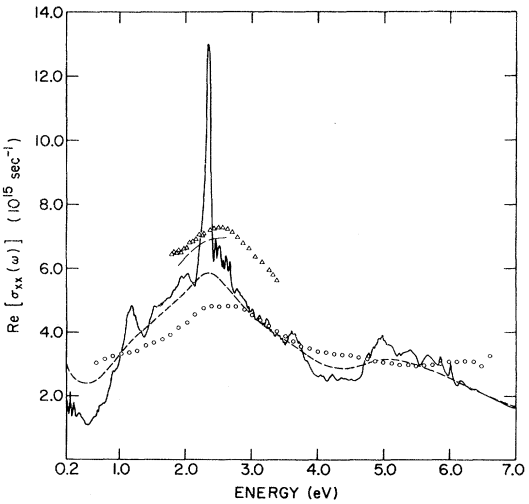

FIG. 8. Real part of the *xx* component of the conductivity tensor from 0.2 to 6 eV. The solid curve is the interband contribution in the sharp limit ($\tau \to \infty$). The dashed curve includes both a Drude term (see text) and a constant relaxation time of 0.3 eV. Experimental results are shown as follows: (long dashed line) Ref. 25; (Δ) Ref. 26; (o) Ref. 27.

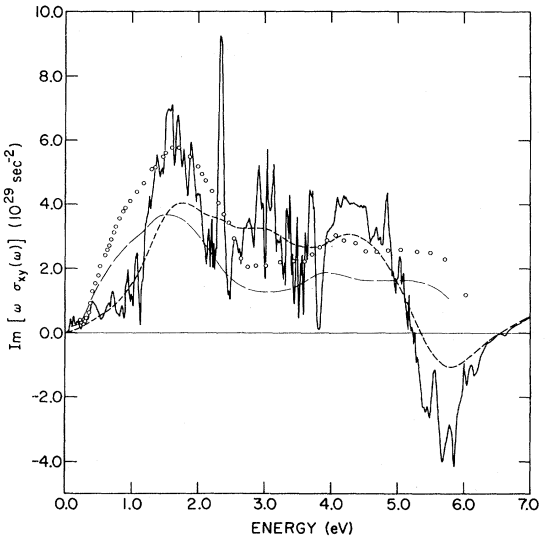

FIG. 9. Imaginary part of $\omega\sigma_{xy}$ from 0 to 6 eV. The solid curve is the interband conductivity in the "sharp" limit; the short dashed curve includes a phenomenological relaxation time $\hbar/\tau = 0.30$ eV. Experimental results are shown as follows; (long dashed line) Ref. 30; (o) Ref. 31.

the momentum matrix elements was included. The numerical integration was based on 729 points in $\frac{1}{16}$th of the Brillouin zone. The reader is referred to Ref. 10 for formulas and additional details.

For the purposes of this calculation, the direction of spin alignment is taken to be [001] and is referred to as "z." Our results for the real part of σ_{xx} from 0.2 to 6 eV are shown in Fig. 8. The solid curve is the interband contribution in the sharp limit ($\tau = \infty$). The dashed curve includes a constant relaxation time $\hbar/\tau = 0.3$ eV and an empirical Drude term with constants ($\sigma_0 = 6.4\times10^{15}$ esu, $\tau' = 9.12\times10^{-15}$ sec) as determined by Lenham and Treherne.[24] Experimental observations of Menzel and Gebhardt,[25] Yolken and Kruger,[26] and Johnson and Christy[27] are shown for comparison. There is reasonably good agreement between the curve containing the relaxation time and the experimental results in regard to the general shape and the position of the maximum, which is the only significant structure observed. We are not aware of observations in the low-energy region ($\hbar\omega < 0.5$ eV) which could show whether sharp structure is present.

The maximum in the computed conductivity near 2.5 eV results from transitions between the nearly parallel pairs of exchange split bands in the vicinity of the zone face (see particularly the directions H-P-N in Fig. 1). The transition would be forbidden in the absence of spin-orbit coupling. Even though the matrix element is relatively small, the joint density of states is quite large, and a large spike in the conductivity is produced. However, at an excitation energy of 2.5 eV, lifetime broadening effects are apparently quite appreciable, and the sharp structure is broadened into a smooth peak. The relaxation time mentioned above, 0.3 eV, seems to reproduce the width of the experimentally observed peak.

If our interpretation of the observed peak in the optical conductivity is correct, it indicates that the band calculation has given approximately the correct spin splitting between bands of predominately majority and minority spins. This contrasts with the situation in nickel, where the calculation yielded an exchange splitting perhaps 60% larger than the actual value (which is, however, not precisely known). We have also pointed out above that agreement between the calculated and experimental Fermi surfaces would be improved in some respects by a reduction of the exchange splitting. We do not have a resolution for this problem at this time.

The absorptive part of the off-diagonal elements of the conductivity tensor can be determined from measurements of the ferromagnetic Kerr effect.[28] This effect involves spin-orbit coupling in an essential way. We have calculated the off-diagonal element σ_{xy} of the conductivity tensor. Our results for $\omega\,\mathrm{Im}(\sigma_{xy})$ are shown in Fig. 9 both in the "sharp" limit ($\tau \to \infty$), and including the same phenomenological relaxation time ($\hbar/\tau = 0.3$ eV) employed for the diagonal portion of the conductivity. We have not included any intraband contribution, which would simply shift the calculated curves by a constant.[29] There is a moderate degree of agreement between theory and observation[30,31] in regard to the magnitude and general trend of the data. We note that the most prominent feature of the experimental results, the peak around 1.7 eV, is also found in our calculations. The transitions which contribute to this peak are not well localized, but appear to come from a fairly large region in the vicinity of N. The minimum present in the calculated conductivity around 5.7 eV seems to result from transitions from the minority-spin lower s-p band to the minority-spin d bands above the Fermi surface.

As in the case of nickel,[10] it appears that a band calculation employing a local exchange potential in combination with spin-orbit coupling is capable of accounting for the general features of the iron Fermi surface and the optical-conductivity tensor. Our previous results have shown that the charge,[1,32] momentum,[33] and spin[1,32] densities are well described. The degree of agreement, in detail, between theory and experiment leaves much to be desired. However, we do not see any evidence on the basis of the properties we have investigated, that many-body effects are unexpectedly large.

ACKNOWLEDGMENTS

We wish to thank Dr. P. B. Johnson for furnishing us with unpublished data and for permission to quote results prior to publication. It is a pleasure to acknowledge many useful discussions with Dr. John Kimball.

---

*Supported in part by the National Science Foundation under Grant No. GH-41417.

[1]R. A. Tawil and J. Callaway, Phys. Rev. B 7, 4242 (1973).
[2]A. V. Gold, L. Hodges, P. T. Panousis, and D. R. Stone, Int. J. Magn. 2, 357 (1971).
[3]D. R. Baraff, Phys. Rev. B 8, 3439 (1973).
[4]R. V. Coleman, R. C. Morris, and D. J. Sellmyer, Phys. Rev. B 8, 317 (1973).
[5]M. M. Angadi, E. Fawcett, and M. Rasolt, Phys. Rev. Lett. 32, 613 (1974).
[6]L. M. Falicov and J. Ruvalds, Phys. Rev. 172, 498 (1968).
[7]A. P. Cracknell, Phys. Rev. B 1, 1261 (1970).
[8]R. Maglic and F. M. Mueller, Int. J. Magn. 1, 289 (1971).
[9]S. Wakoh and J. Yamashita, J. Phys. Soc. Jpn. 21, 1712 (1966).
[10]C. S. Wang and J. Callaway, Phys. Rev. B 9, 4897 (1974).
[11]E. Lafon and C. C. Lin, Phys. Rev. 152, 579 (1966).
[12]A. J. H. Wachters, J. Chem. Phys. 52, 1033 (1970).
[13]J. C. Slater, T. M. Wilson, and J. H. Wood, Phys. Rev. 179, 28 (1969).
[14]W. Kohn and L. J. Sham, Phys. Rev. 140, A 1133 (1965); R. Gaspar, Acta Phys. Hung. 3, 263 (1964).
[15]J. Callaway and J. L. Fry, in *Computational Methods in Band Theory*, edited by P. M. Marcus, J. F. Janak, and A. R. Williams (Plenum, New York, 1971), p. 571.
[16]K. J. Duff and T. P. Das, Phys. Rev. B 3, 1921 (1971).
[17]E. U. Condon and G. H. Shortley, *The Theory of Atomic Spectra* (Cambridge U. P., Cambridge, 1959), Chap. 7.
[18]G. Gilat and C. J. Raubenheimer, Phys. Rev. 144, 390 (1966).
[19]H. Danan, A. Heer, and A. J. P. Meyer, J. Appl. Phys. 39, 669 (1968).
[20]G. I. Rusov, Fiz. Tverd. Tela 9, 196 (1967) [Sov. Phys.-Solid State 9, 146 (1967)].
[21]G. G. Scott, Rev. Mod. Phys. 34, 102 (1962).
[22]M. Dixon, F. E. Hoare, T. M. Holden, and D. E. Moody, Proc. R. Soc. Lond. A 285, 561 (1965).
[23]J. H. Wood, Phys. Rev. 126, 517 (1962).
[24]A. P. Lenham and D. M. Treherne, in *Optical Properties and Electronic Structure of Metals and Alloys*, edited by F. Abeles (North-Holland, Amsterdam, 1966), p. 196.
[25]E. Mensel and J. Gebhardt, Z. Phys. 168, 392 (1962).
[26]H. T. Yolken and J. Kruger, J. Opt. Soc. Am. 55, 842 (1965).
[27]P. B. Johnson and R. W. Christy, Phys. Rev. B 9, 5056 (1974).
[28]P. N. Argyres, Phys. Rev. 97, 334 (1955).
[29]J. L. Erskine and E. A. Stern, Phys. Rev. B 8, 1239 (1973).
[30]J. L. Erskine and E. A. Stern, Phys. Rev. Lett. 30, 1329 (1973).
[31]G. S. Krinchik and V. S. Gushchin, Zh. Eksp. Teor. Fiz. 56, 1833 (1969) [Sov. Phys.-JETP 24, 984 (1969)].
[32]J. Callaway, R. A. Tawil, and C. S. Wang, Phys. Lett. A 46, 161 (1973).
[33]J. Rath, C. S. Wang, R. A. Tawil, and J. Callaway, Phys. Rev. B 8, 5139 (1973).